

An Augmented State SLAM formulation for Multiple Line-of-Sight Features with Millimetre Wave RADAR

Ebi Jose

School of Electrical and Electronic Engineering
Nanyang Technological University
Nanyang Avenue 639798, Singapore.
Email: ebi@pmail.ntu.edu.sg

Martin D. Adams

School of Electrical and Electronic Engineering
Nanyang Technological University
Nanyang Avenue 639798, Singapore.
Email: eadams@ntu.edu.sg

Abstract—Millimetre wave RADAR can penetrate certain non-metallic objects, meaning that multiple line-of-sight objects can sometimes be detected, a property which can be exploited in mobile robot navigation in outdoor unstructured environments. This paper describes a new approach in predicting RADAR range bins which is essential for simultaneous localisation and map building (SLAM) with millimetre wave RADAR.

The first contribution of this paper is a SLAM formulation using an augmented state vector which includes the normalised RADAR cross sections (RCS) and absorption cross sections of features as well as the usual feature Cartesian coordinates. The term “Normalised” is used as the actual RCS is incorporated into a reflectivity parameter. Normalisation results as it is assumed that the sum of this reflectivity parameter and the absorption and transmittance parameters is unity. This is carried out to provide feature rich representations of the environment to significantly aid the data association process in SLAM.

The second contribution is a predictive model of the power-range spectra (often referred to as *range bins*), from differing vehicle locations, for multiple line-of-sight targets. This forms a predicted power-range observation, based on estimates of the augmented SLAM state.

The formulation of power returns from multiple objects down-range is derived and predicted RADAR range spectra are compared with real spectra, recorded outdoors. This prediction of power-range spectra is a step towards a full, RADAR based SLAM framework.

Index Terms—Millimetre Wave RADAR, RADAR cross section, absorption cross section, SLAM formulation, Power-range spectra prediction, multiple line-of-sight targets.

I. INTRODUCTION

MMW RADAR can provide power-range measurements for the environmental imaging required to perform SLAM [1] in dusty, foggy and poorly illuminated environments. Millimetre wave RADAR signals have the ability to penetrate certain non-metallic objects and can provide information on distributed targets that appear in a single observation [2]. Figure 1 shows the received power attenuation of various materials at different RADAR frequencies. This work is conducted with a 77 GHz Frequency Modulated Continuous Wave (FMCW) RADAR which operates in the millimetre wave region of the electro-magnetic spectrum. The 77 GHz frequency is marked

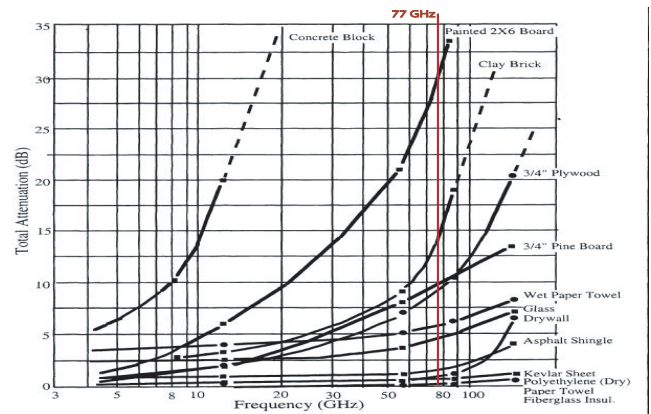
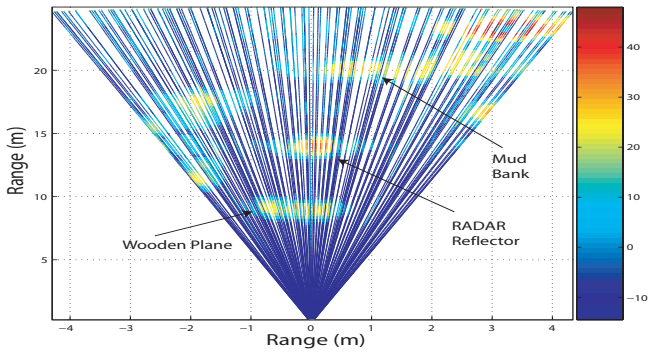
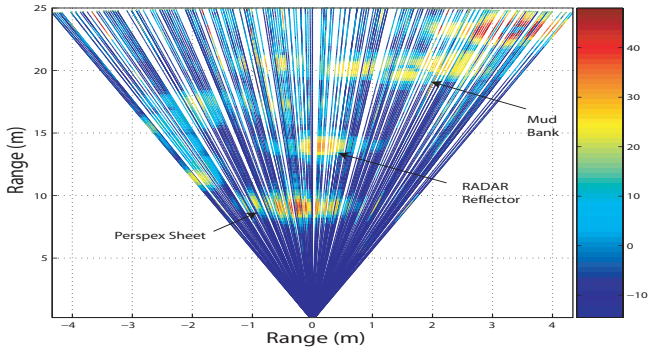


Fig. 1. Attenuation of RADAR waves through various objects as a function of frequency with the 77 GHz frequency marked [2].

in figure 1, where it can be seen that millimeter waves can penetrate various non-metallic materials. For validating the target penetration capability of the RADAR, tests were carried out with two different objects. In the section of the RADAR scan, shown in figure 2(a), a RADAR reflector of RCS 177 m² and a sheet of wood of thickness 0.8cm were placed at ranges of 14m and 8.5m respectively, to visually occlude the reflector from the RADAR. This ensured that no part of the RADAR reflector fell directly within the beam width of the RADAR, so that if it was detected, it must be due to the radio waves penetrating the wood. Figure 2(a) shows the detection of the two features down-range even though, visually, one occludes the other. The experiment was also repeated for a perspex sheet of thickness 0.5 cm (figure 2(b)). The results of object penetration by RADAR waves motivates further development of power spectra prediction with multiple line-of-sight features which is one of the contributions of this paper. For feature based SLAM, it is necessary to predict the target/feature locations reliably, given a prediction of the vehicle/RADAR location. As RADAR can penetrate certain non-metallic objects it can give multiple range information. A method for accurately predicting the power-range spectra (or



(a) A scan of a RADAR reflector of RCS 177 m^2 , 14m from the RADAR and a wooden sheet of thickness 0.8cm visually occluding the reflector from the RADAR. The wooden sheet is 8.5m from the RADAR.



(b) A RADAR reflector of RCS 177 m^2 , 14m from the RADAR and a perspex sheet of thickness 0.5cm, 8.5m from the RADAR. Again, the reflector is visually occluded from the RADAR.

Fig. 2. Initial test results carried out to show the RADAR wave penetration with different objects.

range bins) using the RADAR range equation and knowledge of various noise distributions in the RADAR is explained in this paper.

A mobile robot SLAM problem is then formulated which estimates a state comprising the robot pose, 2D target positions, normalised target RADAR cross sections (RCSs), normalised absorption cross sections and the RADAR power loss, L . The term “Normalised” is used here to indicate that the effect of the actual RCS is incorporated into a reflectivity parameter, Υ_R . Normalisation results as it is assumed that the sum of this reflectivity parameter and the absorption and transmittance parameters is unity. Predicted observations are then formed using the predicted state, the RADAR equation, and a noise analysis, from previous work by the authors. These predicted observations take the form of predicted range-bins which are compared with actual received power/range readings from the RADAR [3], [4]. The RADAR is able to continuously sweep the RADAR wave through 360° in bearing, and acquire entire power-range spectra every 1.8° .

Section II briefly summarises related work, while section III describes the work carried out so far in autonomous navigation with millimetre wave RADAR. A method for predicting RADAR range spectra is explained in section IV based on the RADAR range equation and the knowledge of

the noise statistics. An augmented state vector is introduced in section V where, along with the vehicle and feature positions, normalised RADAR cross sections and absorption cross sections of features are added together with the RADAR losses, L . Finally section VI shows full predicted range spectra and the results are compared with the measured range bins in the initial stages of a simple SLAM formulation.

II. RELATED WORK

Clark [5] presented a method for fusing RADAR readings from different vehicle locations into a two-dimensional representation. This method takes only one range reading per bin which is nearer to the RADAR, discarding all others. In [5] Clark shows a millimetre wave RADAR based navigation system which utilises artificial beacons for localisation and an extended Kalman filter for fusing multiple observations. Manual intervention is required for adjusting the received power threshold as the returned signal power depends on all objects’ RCSs. Foessel shows the usefulness of evidence grids for integrating uncertain and noisy sensor information [6]. In [6], Foessel *et al.* show the development of a RADAR sensor model for certainty grids [7] and also demonstrates the integration of RADAR observations for building three-dimensional outdoor maps. The proposed three-dimensional model by Foessel *et al.* has shortcomings such as the necessity of rigorous probabilistic formulation and difficulties in representing dependencies due to occlusion. In [3], Jose *et al.* shows a method of feature detection from MMW RADAR noisy data.

III. RADAR RANGE SPECTRA PREDICTION

For SLAM, the measurements taken from the RADAR used here are the range, R , bearing, θ and the received power, P_R from the target at range R . One of the contributions of this paper is to predict range bins from new robot positions given an estimate of the vehicle and target states. A new augmented state vector is introduced here which, along with the usual feature coordinates x and y , contains that feature’s normalised RCS, Υ_R and absorption RCS, Υ_a and the RADAR losses, L .

To illustrate this, figure 3 shows a 360° RADAR scan obtained from an outdoor field. Objects in the environment consist of lamp-posts, trees, fences, and concrete steps. The RADAR penetrates some of the non-metallic objects¹, and can observe multiple targets down line. This is shown in figure 4, which is the received power versus range for the particular bearing of 231° marked in figure 3. Multiple targets down range can occur due to either the beam width of the transmitted wave intersecting two or more objects at differing ranges or due to penetration of the waves through certain objects. The RADAR used here is a pencil beam device, with a beam width of 1.8° . This means that multiple returns within the range spectra occur mostly due to penetration. Therefore

¹At 77 GHz the attenuation through paper, fibreglass, plastic, wood, glass, foliage etc. are relatively low while attenuation through brick and concrete is high [2].

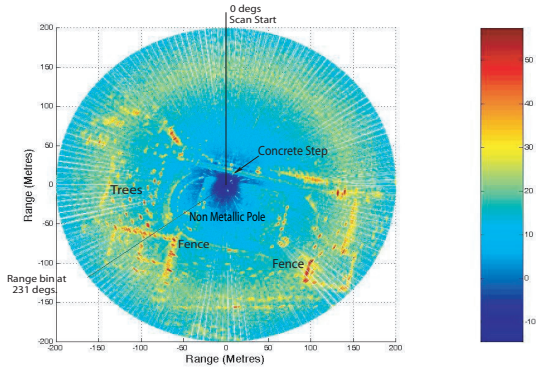


Fig. 3. A 360° RADAR range spectra obtained from an outdoor field, containing a trees, non-metallic poles, fences and concrete walls. The received power value is represented in colour space, as shown by the right hand colour bar, with power units in dB.

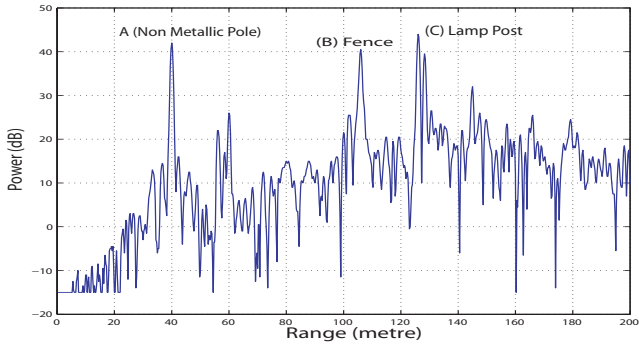


Fig. 4. A single RADAR range bin, recorded at the bearing angle 231 ° shown in figure 3, obtained from the outdoor field with multiple features down range.

a model for predicting entire range spectra, based on target penetration is now given.

IV. RADAR BASED AUGMENTED STATE VECTOR

The state vector consists of the normalised RADAR cross section, Υ_R , absorption cross section, Υ_a and the RADAR loss constants, L , along with the vehicle state and feature locations. The variables, Υ_R , Υ_a and L are assumed unique to a particular feature/RADAR. Hence, this SLAM formulation makes the (very) simplified assumption that all features are stationary and that the changes in the normalised values of RCS and absorption cross sections of features when sensed from different angles, can be modeled using Gaussian random variables v_{Υ_i} . This is a reasonable assumption only for small circular cross sectioned objects such as trees, lamp posts and pillars, however, as will be shown the method produces good results in semi structured environments even for the targets which do not conform to these assumptions. The SLAM formulation here can handle *multiple line-of-sight targets*.

A. Process Model

A simple vehicle predictive state model is assumed with stationary features surrounding it. The vehicle state, $\mathbf{x}_v(k)$ is given by $\mathbf{x}_v(k) = [x(k), y(k), \theta_R(k)]^T$ where $x(k)$, $y(k)$ and

$\theta_R(k)$ are the local position and orientation of the vehicle at time k . The vehicle state, $\mathbf{x}_v(k)$ is propagated to time $(k + 1)$ through a simple steering process model [8].

The model, with control inputs, $\mathbf{u}(k)$ predicts the vehicle state at time $(k + 1)$ together with the uncertainty in vehicle location represented in the covariance matrix $\mathbf{P}(k + 1)$ [9].

$$\mathbf{x}_v(k + 1) = \mathbf{f}(\mathbf{x}_v(k), \mathbf{u}(k)) + \mathbf{v}(k) \quad (1)$$

$\mathbf{u}(k) = [v(k), \alpha(k)]$. $v(k)$ is the velocity of the vehicle at time k and $\alpha(k)$ is the steering angle. In full, the predicted state at time, $(k + 1)$ becomes

$$\begin{bmatrix} \hat{x}(k + 1 | k) \\ \hat{y}(k + 1 | k) \\ \hat{\theta}_R(k + 1 | k) \\ x_{p_I}(k + 1 | k) \\ y_{p_I}(k + 1 | k) \\ \Upsilon_{R_I}(k + 1 | k) \\ \Upsilon_{a_I}(k + 1 | k) \\ \vdots \\ x_{p_N}(k + 1 | k) \\ y_{p_N}(k + 1 | k) \\ \Upsilon_{R_N}(k + 1 | k) \\ \Upsilon_{a_N}(k + 1 | k) \\ L(k + 1 | k) \end{bmatrix} = \begin{bmatrix} \hat{x}(k | k) \\ \hat{y}(k | k) \\ \hat{\theta}_R(k | k) \\ x_{p_I}(k | k) \\ y_{p_I}(k | k) \\ \Upsilon_{R_I}(k | k) \\ \Upsilon_{a_I}(k | k) \\ \vdots \\ x_{p_N}(k | k) \\ y_{p_N}(k | k) \\ \Upsilon_{R_N}(k | k) \\ \Upsilon_{a_N}(k | k) \\ L(k | k) \end{bmatrix} + \begin{bmatrix} \Delta x(k) \\ \Delta y(k) \\ \alpha(k) \\ 0_{p_I} \\ 0_{p_I} \\ 0_{p_I} \\ 0_{p_I} \\ \vdots \\ 0_{p_N} \\ 0_{p_N} \\ 0_{p_N} \\ 0_{p_N} \\ 0 \end{bmatrix} \quad (2)$$

where $\Delta x(k) = v(k)\Delta t \cos(\hat{\theta}_R(k | k) + \alpha(k))$, $\Delta y(k) = v(k)\Delta t \sin(\hat{\theta}_R(k | k) + \alpha(k))$ and Δt is the sampling time.

The augmented state vector is then $\mathbf{x}(k) = [\mathbf{x}_v, \{\mathbf{F}_1, \Upsilon_{R_1}, \Upsilon_{a_1}\}, \dots, \{\mathbf{F}_i, \Upsilon_{R_i}, \Upsilon_{a_i}\}, \dots, \{\mathbf{F}_N, \Upsilon_{R_N}, \Upsilon_{a_N}\}, L]^T$, where \mathbf{x}_v is the vehicle's pose $\mathbf{F}_i = [x_{p_i}, y_{p_i}]^T$ is the i -th feature's location, where $1 \leq i \leq N$. Υ_{R_i} is the normalised RADAR cross section of the i -th feature, Υ_{a_i} is its normalised absorption cross section, L represents the RADAR loss and $\mathbf{v}(k) = [v_v(k), 0_{p_1}, 0_{p_1}, v_{\Upsilon_{R_1}}, v_{\Upsilon_{a_1}}, \dots, 0_{p_i}, 0_{p_i}, v_{\Upsilon_{R_i}}, v_{\Upsilon_{a_i}}, \dots, 0_{p_N}, 0_{p_N}, v_{\Upsilon_{R_N}}, v_{\Upsilon_{a_N}}, 0]^T$.

B. Observation (Measurement) Model

Another contribution of this paper is the formulation of the observation model. The RADAR observation is used to estimate the vehicle's state once the vehicle's pose is predicted. During filter update, the prediction and estimation are fused. For each of the features in the map, the predicted range, $\hat{R}_i(k + 1 | k)$, the RADAR bearing angle, $\hat{\beta}_i(k + 1 | k)$ and the power, $\hat{P}_i(k + 1 | k)$ are to be predicted from the predicted state in equation (2). The predicted range and bearing observations are similar to the ordinary SLAM formulation - *i.e.*

$$\hat{R}_i(k + 1 | k) = \sqrt{[\hat{x}_{p_i}(k + 1 | k) - \hat{x}_R(k + 1 | k)]^2 + [\hat{y}_{p_i}(k + 1 | k) - \hat{y}_R(k + 1 | k)]^2} \quad (3)$$

$$\hat{\beta}_i(k + 1 | k) = \hat{\theta}_R(k + 1 | k) - \tan^{-1} \left[\frac{\hat{y}_{p_i}(k + 1 | k) - \hat{y}_R(k + 1 | k)}{\hat{x}_{p_i}(k + 1 | k) - \hat{x}_R(k + 1 | k)} \right] \quad (4)$$

The predicted power for all targets, such as those in figure 4, is the fundamental difference offered in this paper.

1) *Predicted Power Observation Formulation:* The assumptions made in the predicted power model are as follows.

- The environmental features of interest are assumed to have small circular cross-sections, so that the estimated normalised RADAR cross sections and absorption coefficients are approximately the same in all directions with respect to that feature.
- The measured returned power should be independent of range (due to the built-in range compensation filter). This filter must first be removed or post-filtered to remove its effect, to produce range dependent power returns from all objects [3].
- The beam-width of the RADAR wave does not increase considerably with range.

A target is assumed to affect the incident electro-magnetic radiation in three possible ways:

- 1) A portion of the incident energy Υ_R , $0 \leq \Upsilon_R \leq 1$, is reflected and scattered.
- 2) A portion of the incident energy Υ_a , $0 \leq \Upsilon_a \leq 1$, is absorbed by the target.
- 3) A portion of the incident energy $1 - (\Upsilon_R + \Upsilon_a)$ is further transmitted through the target.

Υ_R is thus referred to as the ‘‘Normalised’’ RADAR cross section. Figure 5 shows a millimetre wave RADAR in an environment with i -features down-range at a particular bearing. The following terms are used in formulating the predicted power observation.

- P_{INCi} = Power incident on the i^{th} feature.
- P_{REFi} = Power reflected from the i^{th} feature.
- P_{TRANi} = Power transmitted through the i^{th} feature.
- P_{INCi1} = Power incident on the first feature which is reflected from the i^{th} feature.
- P_{REFi1} = Power reflected back towards the i^{th} feature from the first feature. This component will not reach the RADAR receiver directly and is not considered in this formulation.
- P_{TRANi1} = Power transmitted through the first feature which is the reflection from the i^{th} feature.

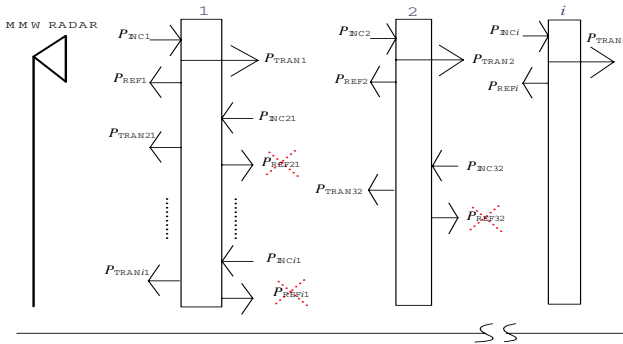


Fig. 5. Power definitions for reflections, absorptions and transmissions for i multiple line-of-sight features.

The power incident at the first feature is given by

$$P_{INC1} = \frac{P_t G A_I}{4\pi R_1^2} \quad (5)$$

where P_t is the power transmitted by the RADAR, G is the antenna gain and R_1 is the distance between RADAR and the first feature and A_I is the area of the object illuminated by the RADAR wave. Let Υ_{R_1} be the normalised RADAR cross section and Υ_{a_1} be the normalised absorption cross section of the first feature. The power received by the RADAR receiver from the first feature is given by $P'_{REF1} = P_{REF1} A_e / (4\pi \hat{R}_1^2)$

$$P'_{REF1} = \frac{P_t G \hat{\Upsilon}_{R_1} A_I}{(4\pi)^2 \hat{R}_1^4} A_e \quad (6)$$

where A_e is the antenna aperture. It is shown in the RADAR literature that $A_e = G\lambda^2/4\pi$ [10]. Substituting for A_e in equation 6, the power return from the first feature is

$$P'_{REF1} = \frac{P_t G^2 \lambda^2 \hat{\Upsilon}_{R_1} A_I}{(4\pi)^3 \hat{R}_1^4} \quad (7)$$

The power P_{TRAN1} that passes through the first feature is given by

$$P_{TRAN1} = \frac{P_t G A_I (1 - [\hat{\Upsilon}_{R_1} + \hat{\Upsilon}_{a_1}])}{(4\pi) \hat{R}_1^2} \quad (8)$$

The power reflected from the second feature, P_{REF2} is given by

$$P_{REF2} = \frac{P_t G A_I^2 \hat{\Upsilon}_{R_2} (1 - [\hat{\Upsilon}_{R_1} + \hat{\Upsilon}_{a_1}])}{(4\pi)^2 \hat{R}_1^2 (\hat{R}_2 - \hat{R}_1)^2} \quad (9)$$

The power then transmitted back to the first feature from the second feature is given by

$$P_{INC21} = \frac{P_t G A_I^3 \hat{\Upsilon}_{R_2} (1 - [\hat{\Upsilon}_{R_1} + \hat{\Upsilon}_{a_1}])}{(4\pi)^3 \hat{R}_1^2 (\hat{R}_2 - \hat{R}_1)^4} \quad (10)$$

The power, P_{INC21} then passes through feature 1 and is given by

$$P_{TRAN21} = P_{INC21} (1 - [\hat{\Upsilon}_{R_1} + \hat{\Upsilon}_{a_1}]) \quad (11)$$

The power returned from the second feature is then $P'_{TRAN21} = P_{TRAN21} A_e / (4\pi \hat{R}_1^2)$

$$P'_{TRAN21} = \frac{P_t G A_I^3 A_e \hat{\Upsilon}_{R_2} (1 - [\hat{\Upsilon}_{R_1} + \hat{\Upsilon}_{a_1}])^2}{(4\pi)^4 \hat{R}_1^4 (\hat{R}_2 - \hat{R}_1)^4} \quad (12)$$

In general, the predicted observed power from the i^{th} feature can be written as

$$\hat{P}'_{TRANi1}(k+1|k) = \frac{K A_I^{(2i-1)} \hat{\Upsilon}_{R_i}(k+1|k)}{(4\pi)^{2i}} \times \frac{\prod_{j=0}^{i-1} [1 - (\hat{\Upsilon}_{R_j}(k+1|k) + \hat{\Upsilon}_{a_j}(k+1|k))]^2}{\prod_{j=0}^{i-1} (\hat{R}_{j+1}(k+1|k) - \hat{R}_j(k+1|k))^4} \quad (13)$$

where $K = P_t G A_e$, $A_e = \frac{G\lambda^2}{4\pi}$, $\hat{\Upsilon}_{R_0} = \hat{\Upsilon}_{a_0} = \hat{R}_0 = 0$ and, for the i -th feature, \hat{R}_i is related to the augmented state by equation 3.

Equations 3, 4 and 13 between them comprise the observation. In order to generate realistic predictions of the range bins, knowledge of the power and range noise distributions is necessary. This has been studied extensively in previous work, and can be found in [3].

The range and power noise are experimentally obtained [3]. The noise in range is the phase noise, which is obtained by observing the range bins containing reflections from objects with different RCSs at different locations. The noise statistics in power is obtained during both target presence and absence.

The angular standard deviation is assumed to be 1° as the RADAR wave is a pencil beam. The observation model is then given by

$$\begin{aligned} \mathbf{z}_i(k+1) &= [\mathbf{R}_i(k+1), \beta_i(k+1), P_i(k+1)]^T + \mathbf{w}_i(k+1) \\ &= \mathbf{h}(\mathbf{x}(k+1)) + \mathbf{w}_i(k+1) \end{aligned} \quad (14)$$

where $\mathbf{z}_i(k+1)$ is the observation, and $\mathbf{w}_i(k+1)$ is the additive observation noise given by

$$\mathbf{w}_i(k+1) = [v_R(k+1)v_\beta(k+1)v_p(k+1)]^T \quad (15)$$

and \mathbf{h} is the non-linear observation function defined by equations 3, 4 and 13.

V. RESULTS

To validate the formulation for realistically predicting multiple line-of-site target range bins, tests using a RADAR unit from Navtech Electronics were carried out. Initially the vehicle was positioned at pose $\mathbf{x}_v(k)$ as demonstrated in figure 6. The full 360° RADAR scan obtained from this

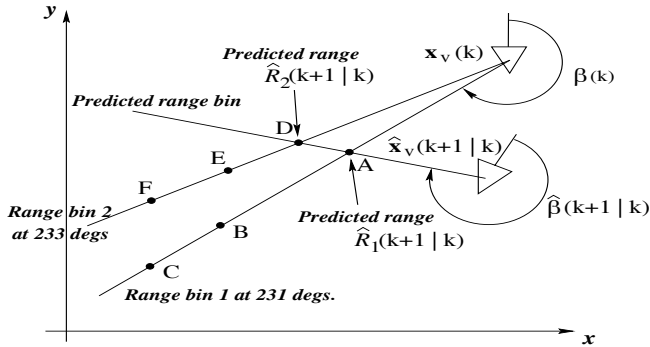


Fig. 6. Vehicle motion and the features observed/predicted. Features observed/predicted down-range at different bearings are marked.

vehicle location is shown in figure 3. Range bins obtained from the initial vehicle location at two different bearing angles are shown in figures 4 and 7. Figure 4 is obtained at azimuth 231° and is indicated by the black line in figure 3. Features in the environment are marked in the figures. The next predicted vehicle location is calculated using the vehicle model and system inputs (equation 2). This corresponds to the new predicted vehicle pose $\hat{\mathbf{x}}_v(k+1|k)$ in figure 6. The range spectra in all directions are then predicted from the new predicted vehicle location. For example, in the range

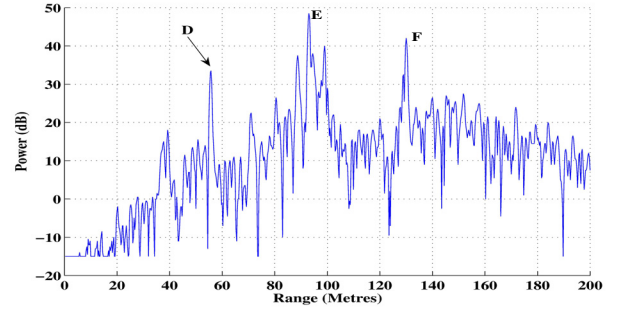


Fig. 7. RADAR Range Spectra (233° azimuth) obtained at the starting robot location. Two features observed down-range are marked.

bin predicted at angle $\hat{\beta}(k+1|k)$ in figure 6, the predicted values for the range, bearing and received power of features A and D are calculated according to equations 3, 4 and 13.

A single range prediction obtained from the predicted vehicle location $\mathbf{x}_v(k+1|k)$ is shown in figure 8 having two features down-range.

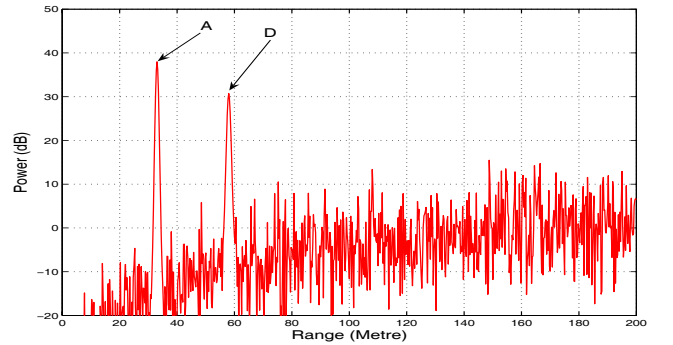


Fig. 8. Predicted RADAR Range Spectra (at 234° bearing) obtained from the predicted vehicle location.

Equation 13 can be used to predict the received power as long as the power bias as a function of range incorporated into the RADAR electronics must be taken into account. This simply requires knowledge of the RADAR's high pass filter circuitry which in an FMCW RADAR compensates for the fourth power of range loss, expected according to the simple RADAR equation [10], [3].

The actual observation is obtained from the next vehicle location and is shown in figure 9 which shows power peaks in close proximity to those predicted in figure 8. The predicted and actual received powers from the target at A are in close agreement in both figures whereas, the predicted value for the received power (30 dB) of the target at 58 metres (feature D in figure 8) is slightly less than the actual received power (38 dB) in figure 9. The discrepancy for feature D can be due to violation of some of the assumptions made in the formulation - in particular that the normalised reflection and absorption cross sections remain constant, independent of the RADAR to target angle of incidence.

Figure 10 shows the results of a chi-squared test to de-

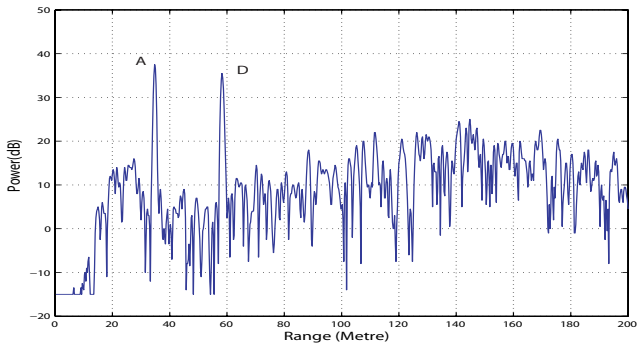


Fig. 9. Actual RADAR Range Spectra (at 234° bearing) obtained at the next robot location. Features observed down-range are marked.

termine any bias or inconsistency in the power-range bin predictions. The difference between the measured and the predicted range bins is plotted together with 99% confidence interval. The value of 99% bound, = ± 16.35 dB, has been found experimentally by recording several noisy power-range bins in target absence (RADAR pointing towards open space) [3]. Close analysis of figure 10 shows that the error has a negative bias. This is due to the approximate assumption of the high pass filter gain. For the RADAR used here, the gain of the high pass filter used in the predicted power-range bins was set to 60 dB/decade². The result shows that this approximation for the high pass filter gain is acceptable, as a large portion of the error plot lies within the 3σ limits.

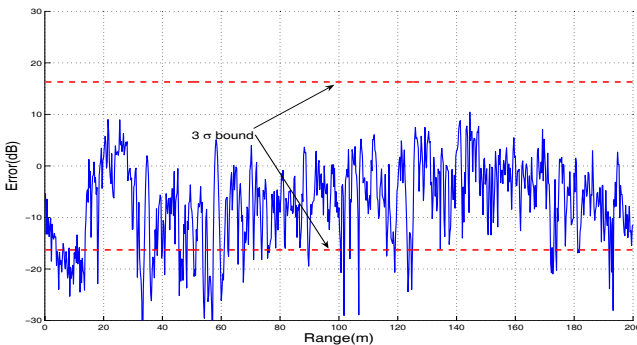


Fig. 10. The difference between predicted and measured range bins containing two features down-range is shown. This error is compared against 3σ noise power bounds.

This formulation and analysis shows the initial stages necessary in implementing an augmented state, feature rich SLAM formulation with millimetre wave RADAR. Future work will address the ease with which data association can be carried out using the multi-dimensional feature state

²Assuming the RADAR range equation to be correct, a high pass filter with a gain of 40 dB/decade should produce a flat power response for particular targets at various ranges. Figure 4, shows a power-range spectrum recorded from the RADAR. It can be seen from figure 4, that the power range response is not flat. For this particular RADAR it makes sense to either determine the bias in the power-range spectra or, model the high pass filter as having a gain of 60 dB/decade, which would better approximate the power-range relationship actually produced in figure 4.

estimates, and a full SLAM implementation in outdoor environments, will be tested.

VI. CONCLUSIONS

This paper describes a new approach in predicting RADAR range bins which is essential for simultaneous localisation and map building (SLAM) with millimetre wave RADAR.

A SLAM formulation using an augmented state vector which includes the normalised RADAR cross sections and absorption cross sections of features, as well as the usual feature Cartesian coordinates, was introduced. This is intended to aid the data association process, so that features need not just be associated based on their Cartesian coordinates, but account can be taken of their estimated normalised reflection and absorption cross sections also.

The second contribution is a predictive model of the form and magnitudes of the power-range spectra from differing vehicle locations, for multiple line-of-sight targets. This forms a predicted power-range observation, based on estimates of the augmented SLAM state.

The formulation of power returns from multiple objects down-range is explained and predicted RADAR range spectra are compared with real spectra, recorded outdoors. This prediction of power-range spectra is a step towards a full, RADAR based SLAM framework.

VII. ACKNOWLEDGEMENTS

This work was funded under the second author's AcRF Grant, RG 10/01, Singapore. We gratefully acknowledge help from SIMTech in the use of their utility vehicle and valuable advice from Graham Brooker (ACFR) and Steve Clark (Navtech Electronics, UK).

REFERENCES

- [1] W.S. Wijesoma, K.R.S. Kodagoda, and A.P. Balasuriya. Road boundary detection and tracking using ladar. In *IEEE Trans. Robotics and Automation*, volume 20, pages 456–464, 2004.
- [2] Jr. Ferris, D.D. and N.C. Currie. Microwave and millimeter-wave systems for wall penetration. *Proceedings of the SPIE - The International Society for Optical Engineering*, 3375:269 – 79, 1998.
- [3] Ebi Jose and Martin D. Adams. Millimetre wave radar spectra simulation and interpretation for outdoor slam. In *International Conference on Robotics and Automation (ICRA)*, New Orleans, USA, April 2004.
- [4] Ebi Jose and Martin D. Adams. Relative radar cross section based feature identification with millimetre wave radar for outdoor slam. In *International Conference on Intelligent Robots and Systems (IROS)*, Sendai, Japan, September 2004.
- [5] Steve Clark and Hugh Durrant-Whyte. Autonomous land vehicle navigation using millimeter wave radar. In *International Conference on Robotics and Automation (ICRA)*, pages 3697–3702, 1998.
- [6] Alex Foessel. *Scene Modeling from Motion-Free Radar Sensing*. PhD thesis, Robotics Institute, Carnegie Mellon University, Pittsburgh, PA, January 2002.
- [7] Sebastian Thrun. Learning occupancy grids with forward models. In *Proceedings of the Conference on Intelligent Robots and Systems*, Hawaii, 2001.
- [8] Guivant J, Nebot E, and Baiker S. Autonomous navigation and map building using laser range sensors in outdoor applications. In *Journal of Robotic Systems*, volume 17, pages 565–283, October 2000.
- [9] Y.Bar-Shalom and T.E.Fortmann. *Tracking and Data Association*. Academic Press, 1988.
- [10] M.I Scolnik. *Introduction to Radar Systems*. McGraw Hill, New York, 1982.